Letter

Dipole-driven multidimensional fusion:
An insightful approach to the formation of superheavy nuclei

T. Cap [1,*] A. Augustyn [1] M. Kowal [1] and K. Siwek-Wilczyńska [2]
[1]*National Centre for Nuclear Research*, Pasteura 7, 02-093 Warsaw, Poland
[2]*Faculty of Physics, Warsaw University*, Pasteura 5, 02-093 Warsaw, Poland

We present an approach to describe the fusion of two heavy ions in which the colliding system has access to a wide spectrum of shapes through the utilization of an auxiliary reference frame and the employment of a multipole expansion of the nuclear radius with the dipole term treated as an actual and leading shape variable. Access to fusion shapes that would otherwise be unattainable is possible by initially placing the origin of the auxiliary reference frame in the neck region between the colliding nuclei. The fusion process is modeled as an unconstrained biased random walk in a four-dimensional deformation space with step probabilities correlated to the density of available states. Deformation energy is calculated using the macroscopic-microscopic method, incorporating rotational energy. The presented approach successfully describes fusion probabilities for reactions involving ^{48}Ca, ^{50}Ti, and ^{54}Cr projectiles with a ^{208}Pb target.

The experimental data show that the cross sections for producing nuclei with atomic numbers $102 \leqslant Z \leqslant 113$ using cold fusion reactions, in which ^{208}Pb and ^{209}Bi targets are bombarded with nuclei of lighter elements, decrease by seven orders of magnitude, from hundreds of nanobarns to the experimentally difficult-to-achieve femtobarn level, as the projectile nucleus changes from ^{48}Ca to ^{70}Zn [1].

Models employed to calculate cross sections for the synthesis of heavy and superheavy nuclei assume that the process occurs in three independent steps: capture of the projectile by the target, fusion, i.e., the formation of an excited compound nucleus, and de-excitation through the emission of neutrons, light charged particles, and γ rays.

The observed decrease in cross section for cold synthesis is attributed to the intermediate stage of the reaction, which represents the most challenging aspect of model calculations. Despite years of dedicated research, there is no consensus on the underlying fusion mechanisms [2]. In calculations, this step is typically parametrized based on measured evaporation residue cross sections, incorporating various assumptions about the process itself. Consequently, predictions for new reactions often differ significantly between models [2,3].

In this Letter, we present an approach that successfully describes experimentally determined fusion probabilities for ^{48}Ca, ^{50}Ti, and ^{54}Cr reactions with a ^{208}Pb target, without relying on measured cross sections or model parameter calibration. The model is based on the random-walk method in a multidimensional deformation space and offers detailed insights into the underlying process. While such an approach has already been employed to describe fission from excited states [4], it is not commonly utilized to describe fusion,

primarily due to difficulties in determining the configuration from which the process initiates and in accessing the required classes of shapes within a single shape parametrization. However, as will be demonstrated, these issues can be resolved through the application of the standard formula for the nuclear radius when an auxiliary reference frame is introduced.

Following Świątecki's work [5], we assume that the fusion process begins when the colliding nuclei overcome the entrance channel barrier and a mononuclear system begins to form. The initial shape configuration, in which the fragments are barely in contact, is situated within the asymmetric fission valley of the compound nucleus. The final configuration that the system needs to reach is highly compact. Describing the smooth transition between these two configurations is possible by utilizing an auxiliary reference frame initially placed at the projectile-target point of contact and employing the standard multipole expansion of the nuclear radius, with the dipole term treated as an actual and leading shape variable. For axially symmetric shapes the nuclear radius $R(\vartheta)$, where ϑ is the polar angle, can be expressed in spherical harmonics, $Y_{\lambda 0}(\vartheta)$, as follows:

$$R(\vartheta) = cR_0 \left\{ 1 + \sum_{\lambda=1}^{\infty} \beta_{\lambda 0} Y_{\lambda 0}(\vartheta) \right\}, \qquad (1)$$

where c is a volume-fixing factor, R_0 is the nuclear radius of the spherical compound nucleus, and $\beta_{\lambda 0}$ are the expansion coefficients describing nuclear deformations.

The dipole variable β_{10} in Eq. (1) is typically omitted. However, as demonstrated in our earlier study [6], the dipole term is more than just a technical parameter for center-of-mass adjustment; it is responsible for modifying the hyperdeformation characteristics of heavy nuclei.

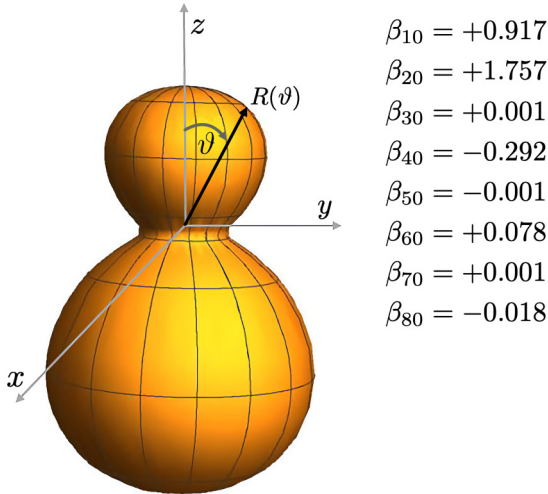_____

*Contact author: tomasz.cap@ncbj.gov.pl

L061603-1

FIG. 1. The initial fusion configuration for the ^{50}Ti + ^{208}Pb system. By placing the reference frame in the zone where the projectile and target nuclei touch, it becomes possible to describe the system's shape during fusion using a multipole expansion of the nuclear radius with only a few deformation parameters.

Including this variable introduces entirely unique and physically meaningful categories of compact shapes. Dipole deformation accumulates a significant amount of energy. Its importance was also demonstrated in [7], where it was shown that including such deformation leads to the disappearance of the previously predicted third deep potential energy minimum in the ^{232}Th nucleus.

To access a wide class of shapes we introduce an auxiliary reference frame whose origin changes its position relative to the center-of-mass frame based on the current deformation of the system. For highly asymmetric shapes, determining the minimum distance between the center of mass and points on the surface within the neck area becomes ambiguous, leading to an indeterminate potential energy for such shapes. Introducing the dipole variable along with an auxiliary reference frame solves this problem and provides us with the capability to describe fusion or fission shapes when both fragments are distinguishable. For axially symmetric shapes, the origin of the auxiliary reference frame shifts exclusively along the axis of symmetry. By initially placing the reference frame's origin at the point of contact between the projectile and target nuclei, we can accurately describe the starting configuration using only a few $\beta_{\lambda 0}$ deformation parameters, the values of which can be obtained by fitting Eq. (1) to a specified shape.

As an example the initial configuration for the ^{50}Ti + ^{208}Pb fusion reaction is shown in Fig. 1. In this case, neither the projectile nor the target is deformed, and the initial shape of the combined system corresponds to two touching spheres with a barely visible neck. The starting values for the $\beta_{\lambda 0}$ parameters are listed in Fig. 1. It is worth noting that the octupole variable β_{30}, typically associated with mass asymmetry, becomes redundant in describing the initial configuration upon introducing the dipole variable. Moreover, it is observed that at significant elongations (quadrupole variable $\beta_{20} > 1$) the neck forms naturally without the need for adding the

hexadecapole variable β_{40}. Among higher-order deformations, only β_{60} has a non-negligible value for the initial configuration. However, as the overall length of the system diminishes, this deformation diminishes as well, and the complete evolution of the system can be effectively described using just four deformation parameters: β_{10}, β_{20}, β_{30}, and β_{40}.

The presented approach proves highly efficient, significantly reducing the number of required deformation parameters and enabling the description of intermediate shapes in the fusion process, including pear-shaped configurations. The concept of using an additional reference frame initially placed at the touching point can probably also be applied to nonaxial shapes by including higher order deformation parameters in Eq. (1). Such an approach could prove useful in describing hot fusion reactions of ^{48}Ca with deformed actinide targets, though this matter requires separate investigation.

Let us denote the set of deformation parameters describing the shape of the composite system at a given moment in the fusion process by β. For a given shape the mass of the system is calculated using the well-established macroscopic-microscopic method detailed in [8]. Here, we will only briefly summarize this method.

The binding energy of the composite system, described by the shape β, is given by the expression

$$E_{\text{tot}}(\beta) = E_{\text{mac}}(\beta) + E_{\text{mic}}(\beta). \tag{2}$$

The microscopic energy, $E_{\text{mic}}(\beta)$, is calculated using the Strutinsky shell correction method applied to the single-particle levels of the deformed Woods-Saxon potential [9]. Pairing energy is accounted for using the Bardeen-Cooper-Schriffer (BCS) theory. The macroscopic component $E_{\text{mac}}(\beta)$ of the binding energy is derived from the liquid-drop formula employing a Yukawa-plus-exponential model, as described in [10].

The shape-dependent binding energy given by Eq. (2) is usually represented as a multidimensional potential energy surface (PES), where $E_{\text{tot}}(\beta)$ is normalized to the macroscopic deformation energy of the spherical shape E_{shpere}. In this study, we will confine the deformation space to four dimensions, represented by the parameters β_{10}, β_{20}, β_{30}, and β_{40} as presented in the Eq. (1). Figure 2 shows a projection of the multidimensional potential energy surface for the ^{258}Rf nucleus formed in the ^{50}Ti + ^{208}Pb reaction onto the β_{20}-β_{30} plane, for fixed values of $\beta_{10} = 0.9$ and $\beta_{40} = 0.0$. The map illustrates one of the possible asymmetric fission valleys located near the place where the nuclear fusion process initiates. The global minimum, representing the compound nucleus configuration, is clearly visible on the map and is preceded by the saddle point.

The likelihood of the system reaching the compound nucleus configuration is significantly influenced by the topology of the potential energy surface, collision energy, and angular momentum. As demonstrated in our recent paper [11], rotational effects play a crucial role in describing fusion probabilities at collision energies above the entrance channel barrier. Specifically, the saddle point, being more compact and possessing a lower moment of inertia, exhibits greater sensitivity to the rise in angular momenta compared to the initial touching configuration of the projectile and target nuclei.
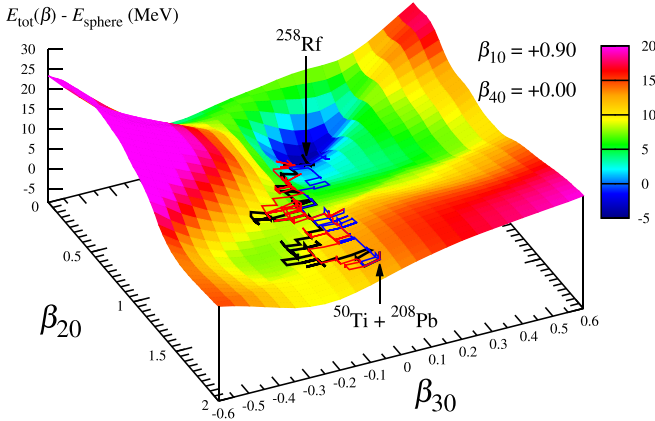
FIG. 2. A fragment of the potential energy map for the ^{258}Rf nucleus calculated within the macroscopic-microscopic model. The map is a projection of a four-dimensional potential energy surface onto the β_{20}-β_{30} plane, with fixed values of $\beta_{10} = 0.9$ and $\beta_{40} = 0.0$. The arrows indicate the approximate starting point of the fusion process for the ^{50}Ti + ^{208}Pb system and the ^{258}Rf compound nucleus configuration. Three examples of fusion trajectories calculated at a compound nucleus excitation energy of 20 MeV and $\ell = 0\hbar$ are presented.

Consequently, the inclusion of rotational energy at every grid point on the potential energy surface is essential.

In low-energy nuclear collisions, the kinetic energy of the impact is rapidly converted into intrinsic excitation energy, mainly due to the intense friction generated during the neck formation process. Therefore, the fusion process can be described within stochastic models in the overdamped regime similar to fission [12]. To describe the merging process, we employ a biased random walk algorithm applied to the four-dimensional potential energy surfaces, treating the β_{10}, β_{20}, β_{30}, and β_{40} deformation parameters as dimensions in which the system can move freely (higher order deformations are neglected). We assume that the process initiates with the contact configuration of the projectile and target nuclei. This assumption limits the applicability of our model primarily to energies above the mean value of the entrance channel barrier B_0. At sub-barrier energies, achieving the touching configuration may not be energetically feasible, leading the system to initiate its evolution from shapes that are more separated.

The probability of transition from one shape to another is determined by the number of available energy levels for a given shape. The Fermi gas model with a constant nuclear level density parameter a is used to calculate the number of energy levels for a point i on the potential energy surface:

$$N_i(\beta_i, \ell) \propto \exp\left(2\sqrt{a\left(E^*_{\max}(\beta_i) - E_{\text{rot}}(\beta_i, \ell)\right)}\right), \quad (3)$$

where $E^*_{\max}(\beta_i)$ represents the maximum excitation energy for a given shape β_i. For nonzero angular momentum this energy is reduced by the collective rotational energy $E_{\text{rot}}(\beta_i, \ell)$ associated with a particular ℓ value, and calculated employing the rigid body moment of inertia.

In the calculations we assume that:

(i) The random walk occurs in a space where the dimensions β_{20}, β_{30}, and β_{40} are unconstrained, while $|\beta_{10}| < 1.6$.

(ii) Only one deformation parameter changes at a time with a step size of 0.05. Given eight possible directions of movement, the probability of transitioning from point i to point j is expressed as $P_{i \rightarrow j}(\ell) = \frac{N_j(\beta_j, \ell)}{\sum_{k=1}^{8} N_k(\beta_k, \ell)}$.

(iii) The random walk process continues until an end condition is met, either fusion or fission.

(iv) Fusion is reached after crossing the saddle point ($\beta_{20} \leqslant 0.3$, $|\beta_{30}| \leqslant 0.2$, and $|\beta_{40}| \leqslant 0.2$). Splitting occurs when the neck thickness is less than 4 fm.

(v) Reaching the end condition for a specific collision energy and angular momentum value defines a single path.

In Fig. 2 we present examples of three fusion paths calculated for the center-of-mass energy $E_{\text{c.m.}} = 189.6$ MeV and angular momentum $\ell = 0\hbar$ projected onto the β_{20}-β_{30} plane (the corresponding excitation energy E^* of the ^{258}Rf* compound nucleus is 20 MeV). Fission paths are usually very short, with the final condition reached after only a slight increase in the quadrupole variable.

The dipole variable plays a crucial role in the fusion process, particularly at the beginning when the system experiences significant elongations. It enables access to highly asymmetric shape classes and facilitates the exploration of otherwise inaccessible natural fusion pathways. The octupole variable starts to engage in the shape description for more compact configurations. The introduction of a hexadecapole variable, describing the neck, adds further complexity to the deformation space. The topology of the potential energy surface reveals intricate correlations between deformation parameters. This emphasizes the significance of providing the system with autonomy to explore a wide spectrum of shapes without imposing artificial distinctions into 'relevant' and 'irrelevant' dimensions, as is often the case with one-dimensional models. The random-walk approach meets these criteria and thus can provide a more profound understanding of the fusion process.

To test the model, we selected three reactions involving ^{48}Ca, ^{50}Ti, and ^{54}Cr projectiles interacting with a ^{208}Pb target, for which fusion probabilities have been determined based on experimental data over a wide range of energies [13–15]. Calculations were performed for compound nucleus excitation energies ranging from 15 to 70 MeV with a 1 MeV step. For a given energy, 10^5 trajectories were calculated for each ℓ value ranging from 0 to the maximum available angular momentum, $\ell_{\max}$, calculated using a sharp cutoff approximation. The partial fusion probability, $P_{\text{fus}}(l)$, is calculated as the ratio of the number of trajectories leading to fusion to the total number of calculated trajectories for a given ℓ. The partial fusion cross section can then be obtained by multiplying $P_{\text{fus}}(l)$ by $\pi \lambdabar^2$, where the squared wavelength $\lambdabar^2 = \frac{\hbar^2}{2\mu E_{\text{c.m.}}}$, and μ is the reduced mass of the colliding system.

In Fig. 3, the ℓ-dependent differential cross section distributions for capture and fusion for the ^{48}Ca + ^{208}Pb system
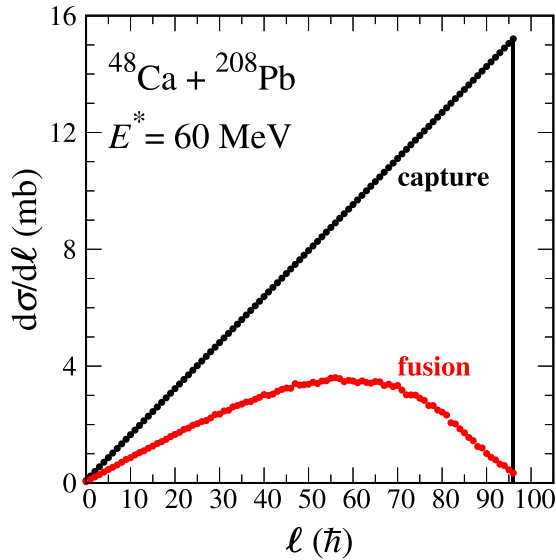
FIG. 3. The ℓ-dependent differential cross section distributions for capture (black) and fusion (red) calculated for ^{48}Ca + ^{208}Pb collisions at a center-of-mass energy of 213.7 MeV. The corresponding excitation energy E^* of the ^{256}No* compound nucleus is 60 MeV. The capture cross section is calculated using a sharp cutoff approximation, while the fusion probability is determined using the random walk method.

are shown as black and red points, respectively. For low values of angular momentum, the differential fusion cross section increases at a slower rate than that observed for the capture process. Additionally, above a certain ℓ value (dependent on the collision energy), a characteristic tail starts to manifest. This change results from the increasing rotational energy. For higher partial waves, the number of available

energy levels [see formula (3)], especially for more compact shapes near the compound nucleus configuration, is limited, reducing the likelihood of reaching these shapes during the fusion process. In particular, this applies to the saddle point, which becomes impassable by the system above a certain value of angular momentum. The incorporation of rotational energy at every grid point of the potential energy surface impacts the trajectories of the random walk, thereby modulating the transmission probability through the multidimensional fusion barrier. The resulting spin distributions are realistic, and the proposed approach enables a detailed investigation of the system's evolution as a function of angular momentum.

To determine the effective fusion probability for a given reaction, one can define the quantity

$$< P_{\text{fus}} >= \frac{1}{(\ell_{\text{max}} + 1)^2} \sum_{\ell=0}^{\ell_{\text{max}}} (2\ell + 1) \times P_{\text{fus}}(\ell), \qquad (4)$$

which represents the fusion probability "averaged" over all angular momenta contributing to the total cross section.

Figure 4 presents a comparison between calculated $< P_{\text{fus}} >$ values and those derived from experimental data for the three investigated reactions. It is important to note that the fusion probability is not a directly measured quantity. The data from Ref. [13] represent an upper limit of the fusion probability and were determined by taking the ratios of estimated fusion cross sections to capture cross sections. The data from Ref. [14] were obtained by comparing experimental mass distributions of fission-like fragments with those expected for compound nucleus fission according to the liquid drop model. Fusion probabilities from Ref. [15] were determined by analyzing angular distributions of fission-like fragments.
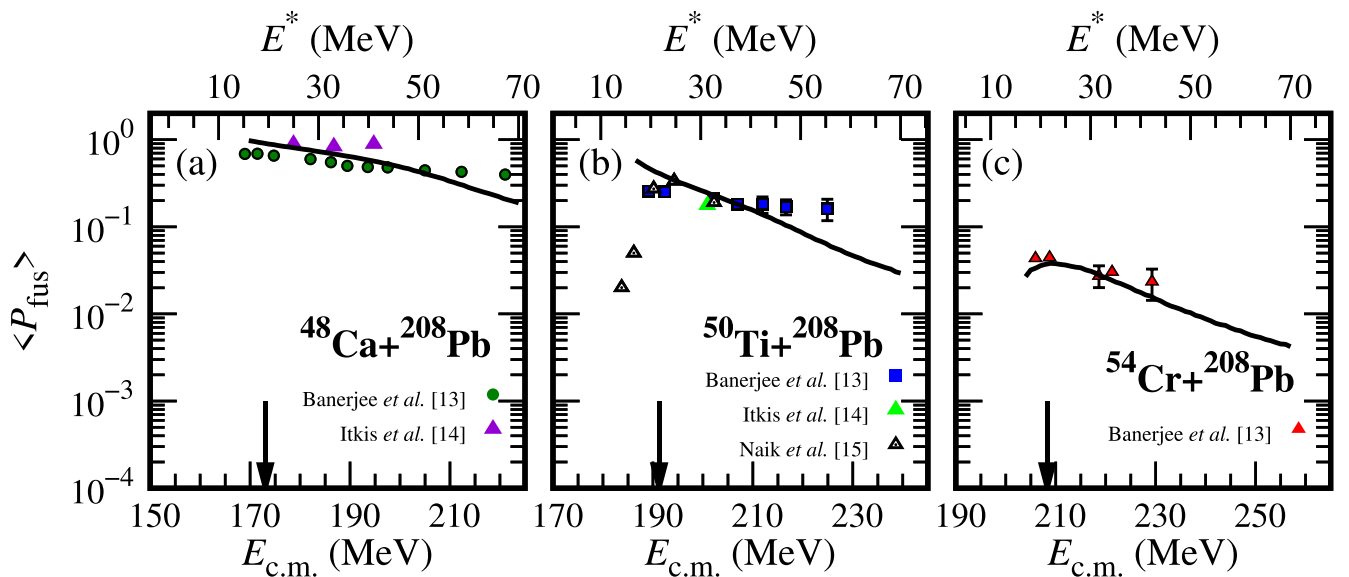

FIG. 4. The averaged fusion probabilities $< P_{\text{fus}} >$ (solid black lines) calculated using the random walk method for the ^{48}Ca + ^{208}Pb, ^{50}Ti + ^{208}Pb, and ^{54}Cr + ^{208}Pb reactions. Experimental data are taken from Refs. [13–15]. The arrows represent the locations of the mean entrance channel barrier B_0 for each reaction (values taken from Ref. [16]).

For reactions involving ^{48}Ca and ^{50}Ti, both target and projectile nuclei are spherical. In the case of the deformed ^{54}Cr projectile, we made the assumption that its shape could be approximated as spherical. It is anticipated that the deformation of ^{54}Cr will have a minor effect, given its relatively lighter mass compared to the target nucleus. Additionally, averaging over all orientations of the projectile and target in the entrance channel is likely to yield a result similar to that of two colliding spherical nuclei.

The model provides a reasonable description of the experimental data, reproducing the effect of a systematic reduction in fusion probabilities associated with the use of heavier projectiles. This effect is a consequence of the deepening and widening of the symmetric fission valley as the atomic number of the compound nucleus increases, making fusion progressively more difficult to achieve as the colliding system's symmetry rises. The observed decrease in fusion probability with increasing beam energy for all reactions can be linked to a critical angular momentum threshold. This effect becomes more pronounced at higher energies, when the denominator in Eq. (4) grows faster than the sum of the partial waves contributing to fusion.

The results presented in this Letter demonstrate that an insightful description of superheavy element formation can be achieved using a simple random-walk method, without the need for model parameter calibration based on experimental data. However, it is necessary to ensure, that the system has access to a wide range of shapes, and the random walk proceeds on a multidimensional potential energy surface that accounts for shell effects and rotational energy.

[1] S. Hofmann, S. N. Dmitriev, C. Fahlander, J. M. Gates, J. B. Roberto, and H. Sakai, On the discovery of new elements (IUPAC/IUPAP report), Pure Appl. Chem. **92**, 1387 (2020).

[2] W. Loveland, An experimentalist's view of the uncertainties in understanding heavy element synthesis, Euro. Phys. J. A **51**, 120 (2015).

[3] X. J. Bao, Fusion dynamics of low-energy heavy-ion collisions for production of superheavy nuclei, Front. Phys. **8**, 14 (2020).

[4] M. Albertsson, B. G. Carlsson, T. Døssing, P. Möller, J. Randrup, and S. Åberg, Super-short fission mode in fermium isotopes, Phys. Rev. C **104**, 064616 (2021).

[5] W. Swiatecki and S. Bjørnholm, Fission and fusion dynamics, Phys. Rep. **4**, 325 (1972).

[6] M. Kowal and J. Skalski, Examination of the existence of third, hyperdeformed minima in actinide nuclei, Phys. Rev. C **85**, 061302(R) (2012).

[7] P. Jachimowicz, M. Kowal, and J. Skalski, Eight-dimensional calculations of the third barrier in ^{232}Th, Phys. Rev. C **87**, 044308 (2013).

[8] P. Jachimowicz, M. Kowal, and J. Skalski, Properties of heaviest nuclei with $98 \leqslant Z \leqslant 126$ and $134 \leqslant N \leqslant 192$, At. Data Nucl. Data Tables **138**, 101393 (2021).

[9] S. Cwiok, J. Dudek, W. Nazarewicz, J. Skalski, and T. Werner, Single-particle energies, wave functions, quadrupole moments and g-factors in an axially deformed woods-saxon potential with applications to the two-centre-type nuclear problems, Comput. Phys. Commun. **46**, 379 (1987).

[10] H. J. Krappe, J. R. Nix, and A. J. Sierk, Unified nuclear potential for heavy-ion elastic scattering, fusion, fission, and ground-state masses and deformations, Phys. Rev. C **20**, 992 (1979).

[11] T. Cap, M. Kowal, and K. Siwek-Wilczyńska, Diffusion as a possible mechanism controlling the production of superheavy nuclei in cold fusion reactions, Phys. Rev. C **105**, L051601 (2022).

[12] M. Albertsson, Nuclear fission and fusion in a random-walk model, Ph.D. Thesis, Lund University, 2021, arXiv:2207.04919.

[13] K. Banerjee, D. J. Hinde, M. Dasgupta, E. C. Simpson, D. Y. Jeung, C. Simenel, B. M. A. Swinton-Bland, E. Williams, I. P. Carter, K. J. Cook, H. M. David, C. E. Düllmann, J. Khuyagbaatar, B. Kindler, B. Lommel, E. Prasad, C. Sengupta, J. F. Smith, K. Vo-Phuoc, J. Walshe *et al.*, Mechanisms suppressing superheavy element yields in cold fusion reactions, Phys. Rev. Lett. **122**, 232503 (2019).

[14] M. Itkis, G. Knyazheva, I. Itkis, and E. Kozulin, Experimental investigation of cross sections for the production of heavy and superheavy nuclei, Euro. Phys. J. A **58**, 178 (2022).

[15] R. S. Naik, W. Loveland, P. H. Sprunger, A. M. Vinodkumar, D. Peterson, C. L. Jiang, S. Zhu, X. Tang, E. F. Moore, and P. Chowdhury, Measurement of the fusion probability P_{CN} for the reaction of ^{50}Ti with ^{208}Pb, Phys. Rev. C **76**, 054604 (2007).

[16] T. Cap, K. Siwek-Wilczyńska, and J. Wilczyński, Nucleus-nucleus cold fusion reactions analyzed with the *l*-dependent "fusion by diffusion" model, Phys. Rev. C **83**, 054602 (2011).